Journal of Superconductivity and Novel Magnetism (2019) 32:3563–3568
https://doi.org/10.1007/s10948-019-5132-2

ORIGINAL PAPER

Structure and Magnetic Properties of the Ti-Doped Pyrochlore Molybdate $Y_2Mo_{2(1-x)}Ti_{2x}O_7$

Yao Ying [1,2] · Wei Zhang [1,2] · Jing Yu [1,2] · Liang Qiao [1,2] · Jingwu Zheng [1,2] · Wangchang Li [1,2] · Juan Li [1,2] · Wei Cai [1,2] · Shenglei Che [1,2]

Received: 19 February 2019 / Accepted: 2 May 2019 / Published online: 15 May 2019

Abstract
The structural, heat capacity, and magnetic properties of $Y_2Mo_{2(1-x)}Ti_{2x}O_7$ were investigated in this work. $Y_2Mo_{2(1-x)}Ti_{2x}O_7$ maintains the pyrochlore structure, but lattice constants are observed to decrease continuously with the Ti^{4+} doping. The magnetic measurements indicate a magnetic phase transition at low temperature for all Ti-doped samples, and the Ti^{4+} doping suppresses the transition temperature. This is ascribed to the diluted effect of nonmagnetic Ti^{4+} substitution of magnetic Mo^{4+}. The heat capacity data confirm that the low-temperature magnetic phase is spin glass in the Ti^{4+}-doped $Y_2Mo_{2(1-x)}Ti_{2x}O_7$ system. The M(H) data reveals the coexistence of antiferromagnetic and ferromagnetic interactions at low temperatures.

Keywords Pyrochlore · Frustrated antiferromagnet · Spin glass

1 Introduction

Pyrochlore oxides have attracted a lot of scientific interest over the past two decades [1–4]. In pyrochlore oxides $A_2B_2O_7$, the rare earth cations and the transition metal cations generally occupy A and B sites, respectively. And the A- and B-site cations form the three-dimension array of corner-shared tetrahedra, respectively. When magnetic metal cations with the inherent antiferromagnetic (AFM) interaction occupy the vertexes of tetrahedra, spins encounter the magnetic frustration. This spin frustration originating from the structure leads to highly degenerate ground states. In some geometrically frustrated antiferromagnets, the degenerate magnetic ground states are lifted by the internal or external factors such as the lattice distortion, the strain, the next-nearest-neighbor interaction, and the ionic doping, which generates a rich variety of magnetic phases including spin glass, spin liquid, spin ice, antiferromagnetism [5–7].

In $Y_2Mo_2O_7$, nonmagnetic Y^{3+} and magnetic Mo^{4+} ions occupy A and B sites, respectively. The magnetic interaction between the nearest neighbor Mo^{4+} ions at B sites is AFM, so the magnetic Mo^{4+} ions in $Y_2Mo_2O_7$ meet the geometrical spin frustration [8]. In the past years, physical properties of $Y_2Mo_2O_7$ and its doping compounds have been investigated in some references [9–11]. It has been established that $Y_2Mo_2O_7$ behaves as a nearly ideal spin glass from nonlinear susceptibility, heat capacity, AC susceptibility, elastic and inelastic neutron scattering, muon-spin relaxation, and neutron spin echo data [10–13]. The other metal ions doping in $Y_2Mo_2O_7$ would change magnetic property due to the change of structure and generation of chemical disorder [14]. The magnetic property in the Ti^{4+}-doped $Y_2Mo_2O_7$ was investigated in reference [15]. In this work, the effect of Ti^{4+} doping in $Y_2Mo_2O_7$ was investigated. The Ti^{4+} doping does not change the structure except slightly increasing the lattice constant in the system. Spin glass is confirmed to persist in the Ti^{4+}-doped $Y_2Mo_2O_7$, but the transition temperature is suppressed with the Ti^{4+} doping.

2 Experimental

Polycrystalline samples of $Y_2Mo_{2(1-x)}Ti_{2x}O_7$ were prepared by using the standard solid-state method. Firstly, the stoichiometric reactants of Y_2O_3 (99.99 wt%), MoO_2 (99 wt%), and TiO_2 (99.99 wt%) were thoroughly mixed. Then the mixtures

✉ Yao Ying
yying@zjut.edu.cn

✉ Shenglei Che
cheshenglei@zjut.edu.cn

[1] College of Materials Science and Engineering, Zhejiang University of Technology, Hangzhou 310014, China

[2] Research Center of Magnetic and Electronic Materials, Zhejiang University of Technology, Hangzhou 310014, China

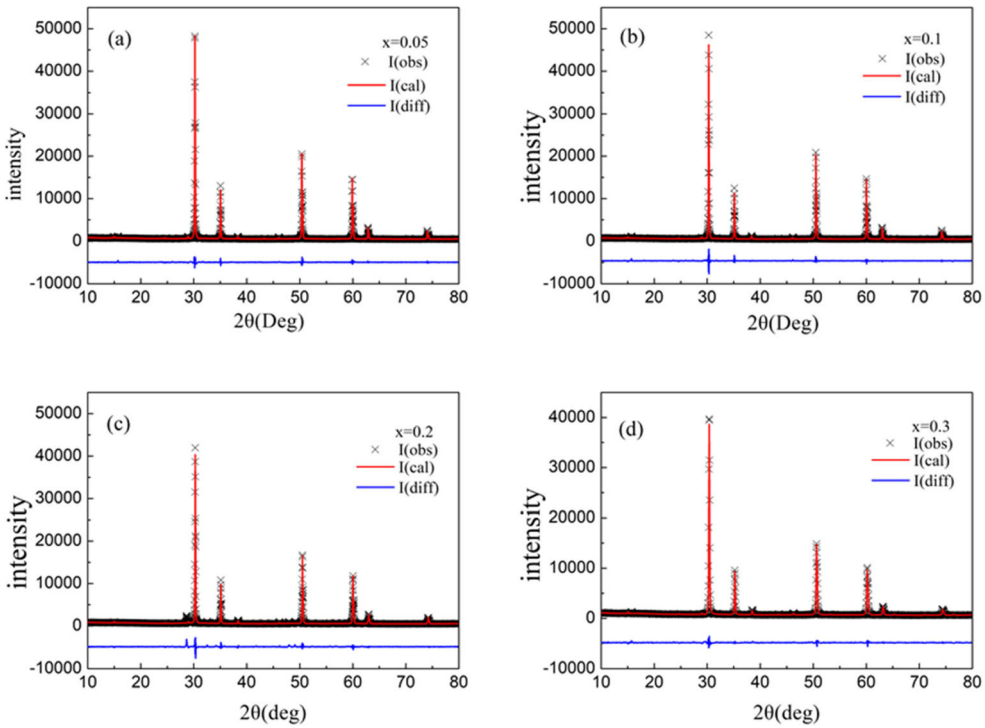

Fig. 1 The XRD data along with Rietveld analysis are shown for $Y_2Mo_{2(1-x)}Ti_{2x}O_7$ with $x = 0.05$, 0.10, 0.20, and 0.30

were pressed into sheets and pre-fired at 1073 K under the flowing N_2. Finally, they were sintered at 1523 K under the same atmosphere with the intermediate grinding. The structure was checked by using the x-ray diffractometer (XRD) with the Cu K_α radiation at room temperature. The XRD data were recorded in the 2θ range from 20° to 80°. The XRD data have been analyzed using Rietveld refinement program (GSAS). The FRIR and Raman spectra were employed to check the change of microstructure in the Ti^{4+}-doped samples. The magnetic properties were measured by employing a superconducting quantum interference device magnetometer. Temperature dependence of magnetization was measured in the zero-field-cooling (ZFC) and the field-cooling (FC) modes under the magnetic field of 100 Oe. The AC susceptibilities at different frequencies were measured at the zero DC magnetic field and a constant AC field of 3.5 Oe from 4 to 200 K. The heat capacity at low temperatures was measured by using physical properties measurement system.

3 Results and Discussion

The experimental and the Rietveld refined XRD data of $Y_2Mo_{2(1-x)}Ti_{2x}O_7$ with $x = 0.05$, 0.10, 0.20, and 0.30 at room temperature were shown in Fig. 1. All $Y_2Mo_{2(1-x)}Ti_{2x}O_7$ samples present in the cubic phase with Fd3m symmetry and no impurity peaks are observed, which indicates that the Ti^{4+} doping does not change the crystal structure in this series of samples. Compared with the standard XRD spectra of $Y_2Mo_2O_7$, the (222) peaks of $Y_2Mo_{2(1-x)}Ti_{2x}O_7$ with $x =$ 0.05, 0.10, 0.20, and 0.30 shift − 0.004°, + 0.053°, + 0.144°, and + 0.155°. For $x = 0.05$, the (222) peak unexpectedly and slightly shifts to the low degree, which may ascribe to measurement inaccuracy from the large measurement step (0.033° per step). The Ti^{4+} doping shifts the (222) peak to the high degree, which means that the lattice constant becomes small. The experimental XRD data for all samples is well simulated by the Rietveld refinement. As shown in Table 1, the lattice constant (D) for $Y_2Mo_{2(1-x)}Ti_{2x}O_7$ decreases monotonically

Table 1 Structural parameters from the Rietveld refinement of XRD data for $Y_2Mo_{2(1-x)}Ti_{2x}O_7$ with $x = 0.05$, 0.10, 0.20, and 0.30 at room temperature

	D (Å)	R_{WP} (%)	R_P (%)	χ^2
$Y_2Mo_{1.90}Ti_{0.10}O_7$	10.2291 (4)	5.76	4.21	2.828
$Y_2Mo_{1.80}Ti_{0.20}O_7$	10.2140 (7)	5.85	4.35	2.826
$Y_2Mo_{1.60}Ti_{0.40}O_7$	10.2138 (3)	5.04	4.29	2.835
$Y_2Mo_{1.40}Ti_{0.60}O_7$	10.1961 (3)	5.53	4.08	3.100

Table 2 The bond lengths between different ions from Rietveld refinements for $Y_2Mo_{2(1-x)}Ti_{2x}O_7$ with $x = 0.05$, 0.10, 0.20, and 0.30

	$x = 0.05$	$x = 0.1$	$x = 0.2$	$x = 0.3$
Y-Y (Å)	3.616	3.611	3.610	3.605
Y-O1 (Å)	2.417	2.400	2.342	2.424
Y-O2 (Å)	2.215	2.211	2.211	2.208
Mo-O1 (Å)	2.044	2.051	2.094	2.028
Ti-O (Å)	1.881	1.901	1.910	2.100

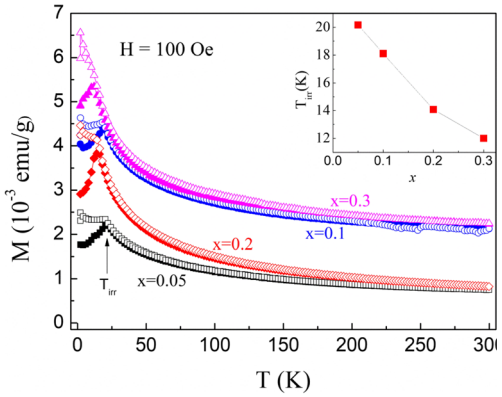

Fig. 2 Temperature-dependent magnetization of $Y_2Mo_{2(1-x)}Ti_{2x}O_7$ under the field of 100 Oe. Filled and unfilled symbols represent the ZFC and FC data, respectively. The inset shows the variation of irreversibility temperature with Ti^{4+} substitution

upon the substitution of Ti^{4+}. This is due to that the ionic radius of Ti^{4+} (0.605 Å) is smaller than that of Mo^{4+} (0.65 Å). The bond lengths between different ions from Rietveld refinements for $Y_2Mo_{2(1-x)}Ti_{2x}O_7$ are shown in Table 2. When Ti^{4+} substitutes Mo^{4+}, the bond lengths between most different ions in $Y_2Mo_{2(1-x)}Ti_{2x}O_7$ vary slightly ($\leq 3.3\%$) except the Ti–O bond (up to 12%). The large change of the Ti–O bond length is related with the microstructure crystalline distortion resulting from the different ionic radii between Mo^{4+} and Ti^{4+}.

Figure 2 shows magnetization as a function of temperature [$M(T)$] for $Y_2Mo_{2(1-x)}Ti_{2x}O_7$ measured under 100-Oe magnetic field. The ZFC and FC $M(T)$ curves are coincident in the high-temperature region and show irreversible at low temperatures. The irreversibility temperature (T_{irr}) of $Y_2Mo_{2(1-x)}Ti_{2x}O_7$ is 20.2, 18.1, 14.1, and 12.0 K for $x = 0.05$, 010, 0.20, and 0.30, respectively. The inset of Fig. 2 exhibits that T_{irr} decreases almost linearly with the doping content of Ti^{4+}. Obviously, the doping of Ti^{4+} suppresses the irreversibility temperature. In $Y_2Mo_2O_7$, the observance of magnetic irreversibility is considered to originate from the thermodynamic spin glass [16, 17]. The generation of spin glass in $Y_2Mo_2O_7$

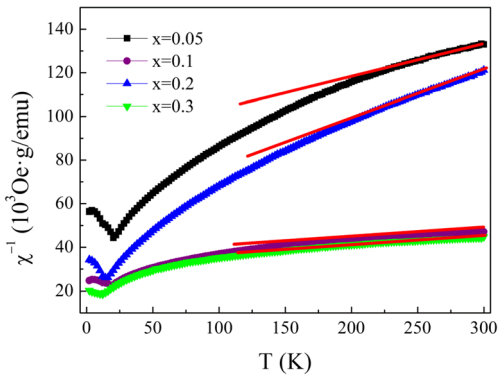

Fig. 3 Temperature-dependent inverse susceptibility deduced from magnetization data of $Y_2Mo_{2(1-x)}Ti_{2x}O_7$ with $x = 0.05$, 0.10, 0.20, and 0.30. The solid lines show the fitting curves with the Curie-Weiss law

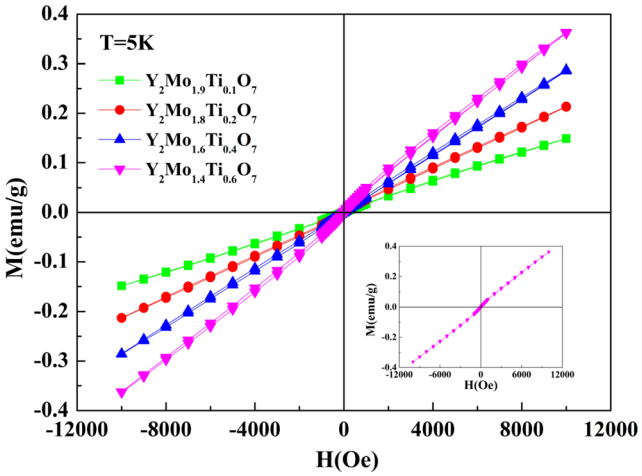

Fig. 4 Magnetic field–dependent magnetization of $Y_2Mo_{2(1-x)}Ti_{2x}O_7$ at 5 K. The inset shows the detailed M(H) curves of $Y_2Mo_{1.40}Ti_{0.60}O_7$

is also confirmed by neutron powder diffraction, the heat capacity, and density functional theory calculations, and suggested to be the results of the spin-orbital coupling and random fluctuations in the Mo environment at the local level [18]. However, magnetic irreversibility behavior is also found in the antiferromagnetic and ferromagnetic systems. So, it could not be concluded that spin glass occurs in the Ti^{4+}-doped $Y_2Mo_{2(1-x)}Ti_{2x}O_7$ system. Temperature dependence of the inverse magnetic susceptibility [$\chi^{-1} = (M/H)^{-1}$] is shown in Fig. 3. The curves are fitted through the Curie-Weiss law $\chi = C/(T - \theta_{CW})$, where C is the Curie constant and θ_{CW} is the Curie-Weiss temperature. The obtained θ_{CW}s for all samples are all negative, which indicates that the main magnetic interaction in $Y_2Mo_{2(1-x)}Ti_{2x}O_7$ is antiferromagnetic.

To further clarify the magnetic state in the $Y_2Mo_{2(1-x)}Ti_{2x}O_7$ system, we studied the isothermal magnetization as a function of a magnetic field [$M(H)$] measured at 5 K for $Y_2Mo_{2(1-x)}Ti_{2x}O_7$ (Fig. 4). The $M(H)$ curves show almost linear behavior, which reflects the strong AFM interaction in this series of samples. But the $M(H)$ curves also show a slight magnetic hysteresis in the low-field region. The typical $M(H)$ curve of $x = 0.20$ as shown in the inset of Fig. 4. The magnetic hysteresis indicates that there is a weak ferromagnetic (FM)

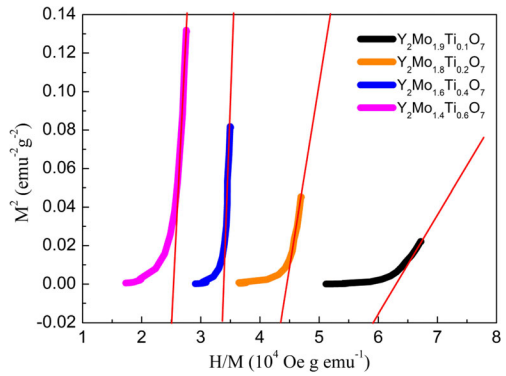

Fig. 5 The Arrott plot (M^2 vs H/M) of $Y_2Mo_{2(1-x)}Ti_{2x}O_7$

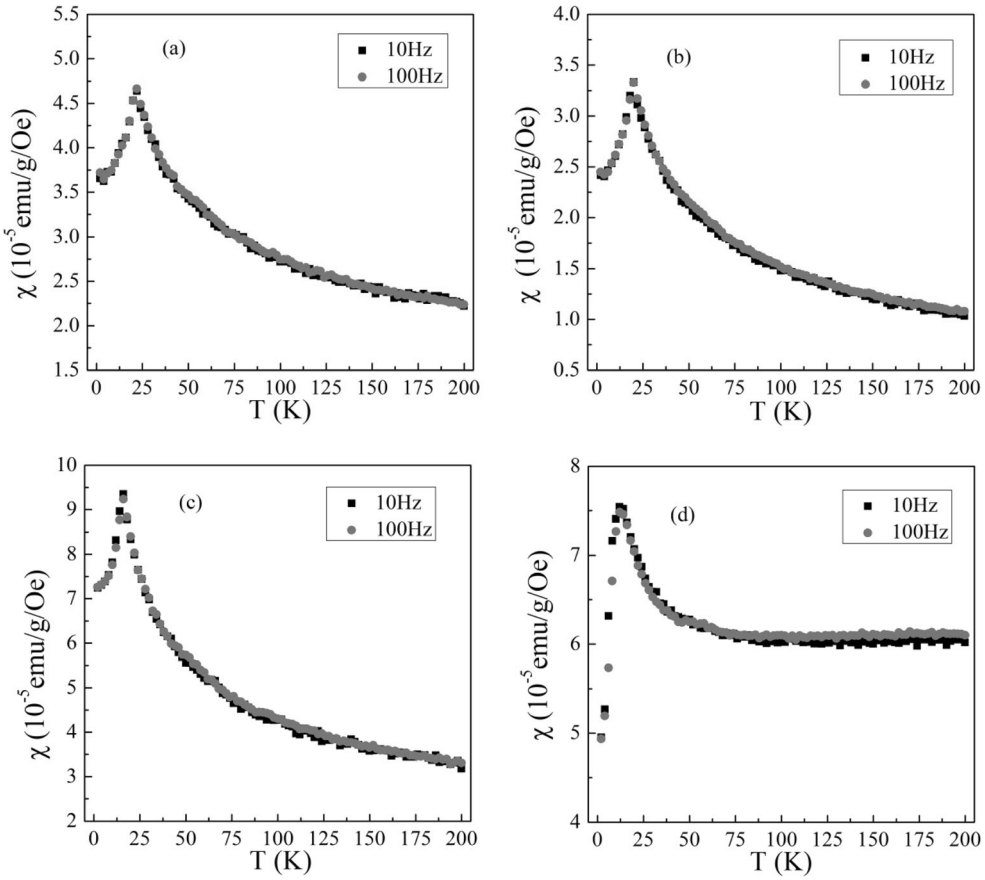

Fig. 6 The real part of the AC susceptibility $Y_2Mo_{2(1-x)}Ti_{2x}O_7$ with x = **a** 0.05, **b** 0.10, **c** 0.20, and **d** 0.30 at the frequency of 10 Hz and 100 Hz

interaction in the system. Figure 5 shows the corresponding Arrott plot (M^2 vs H/M) from the $M(H)$ data [19]. For the materials with spontaneous magnetization, the Arrott plot will give a positive intercept in the high-field regime. On the other hand, a negative intercept in the Arrott plot implies an antiferromagnetic state [19, 20]. As seen in Fig. 5, the intercepts for all samples are negative, which indicates that the AFM interaction is predominated rather than the FM interaction in $Y_2Mo_{2(1-x)}Ti_{2x}O_7$. Therefore, the AFM interaction is predominated but the weak FM interaction also exists in $Y_2Mo_{2(1-x)}Ti_{2x}O_7$.

The coexistence of the AFM and FM interactions in this series of samples would be possible to induce spin glass in the system. To demonstrate whether or not spin glass occurs in $Y_2Mo_{2(1-x)}Ti_{2x}O_7$, we further measured temperature dependence of AC susceptibility under zero DC magnetic field and a constant AC field of 3.5 Oe from 4 to 200 K with different frequencies (f) of 10 Hz and 100 Hz. The real part of AC susceptibility curves [$\chi'(T)$] with different frequencies are shown in Fig. 6. A pronounced peak is observed in the $\chi'(T)$ curves for all samples, and the corresponding temperature is the transition temperature. When frequency change from 10 to 100 Hz, the $\chi'(T)$ curve at 100 Hz is coincident with that of 10 Hz and no peak shift is found for each sample. In a conventional spin glass, when increasing frequency, peak shifts to a higher temperature [8]. But in the $Y_2Mo_{2(1-x)}Ti_{2x}O_7$, no peak shift is found, which is unlike the conventional spin glass. In some spin glass system, the behavior of peak shift could not be detected due to that this shift is smaller than the measurement accuracy. Therefore, the spin glass could not be excluded. The transition temperature obtained from the AC susceptibility is 22, 20, 16, and 14 K for x = 0.05, 0.10, 0.20, and 0.30, respectively.

We further made the heat capacity measurements as a function of temperature [$C_p(T)$] for $Y_2Mo_{2(1-x)}Ti_{2x}O_7$ with x = 0.05, 0.10, 0.20, and 0.30, shown in Fig. 7. The measured $C_p(T)$ curves of $Y_2Mo_{2(1-x)}Ti_{2x}O_7$ (x = 0.05, 0.10, 0.20, and 0.30) is similar to that of $Y_2Mo_2O_7$ [18]. To get the magnetic specific heat, $Y_2Ti_2O_7$ was used as a subtraction from the lattice contribution at low temperatures because $Y_2Mo_2O_7$ presents a similar crystalline structure to $Y_2Ti_2O_7$. Figure 8 shows temperature dependence of the magnetic specific heat [$C_m(T)$] of $Y_2Mo_{2(1-x)}Ti_{2x}O_7$ (x = 0.05, 0.10, 0.20, and 0.30). A broad peak is observed at the transition temperature for all samples. Especially, the magnetic specific heat in the low-temperature region exhibits linear behavior. This phenomenon suggests a constant density of states of the low-temperature magnetic excitations and it is also claimed to be a common feature of spin glass [11, 21, 22]. A broad magnetic specific heat also extends up to high temperatures, which indicates that

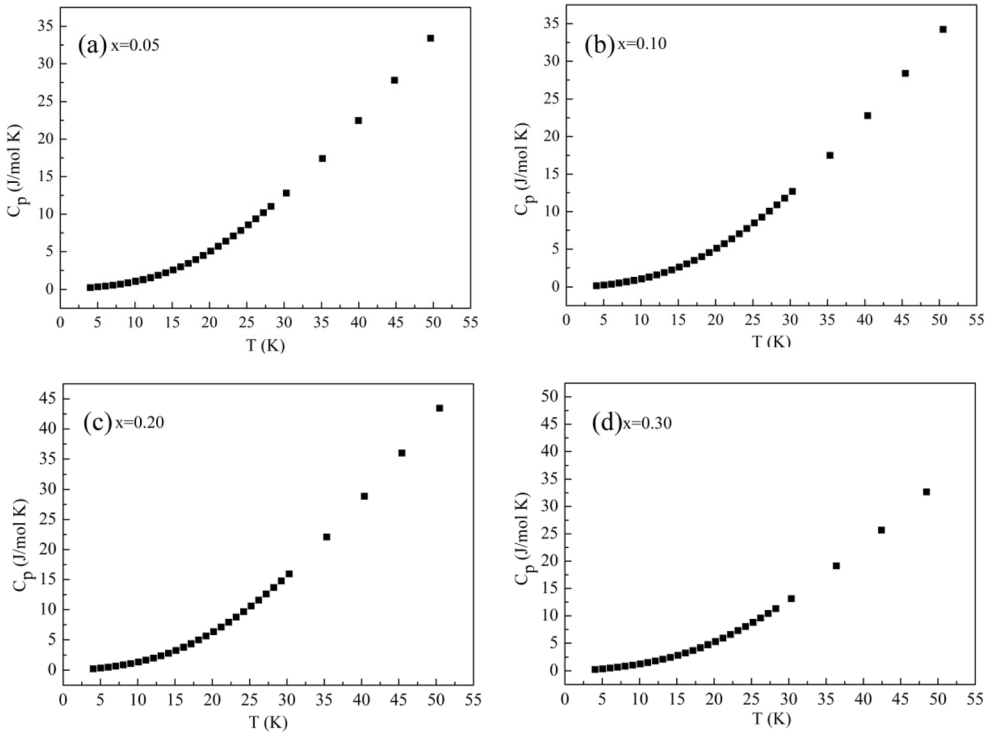

Fig. 7 The measured specific heat of $Y_2Mo_{2(1-x)}Ti_{2x}O_7$ with x = 0.05, 0.10, 0.20, and 0.30 at low temperatures

short-range order contributions persist at the high temperatures [11]. This also confirms spin glass. The coexistence of AFM and FM interactions in the frustrated magnet may be the origin of spin glass in this series of samples.

4 Conclusion

In summary, we have investigated the structural, heat capacity, and magnetic properties of the pyrochlore $Y_2Mo_{2(1-x)}Ti_{2x}O_7$. No structural phase transition is induced, but the lattice constant decreases continuously with Ti^{4+} doping. Spin glass persists in the Ti^{4+}-doped $Y_2Mo_2O_7$ in the low-temperature region. The Ti^{4+} doping suppresses the transition temperature.

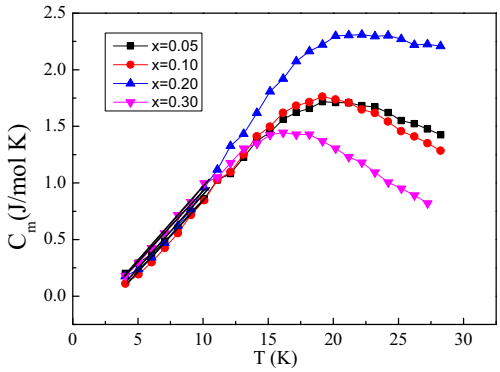

Fig. 8 Magnetic specific heat of $Y_2Mo_{2(1-x)}Ti_{2x}O_7$ with x = 0.05, 0.10, 0.20, and 0.30 at low temperatures. The solid lines show the linear fitting curves in the low-temperature region

This is ascribed to the diluted effect of nonmagnetic Ti^{4+} substitution of magnetic Mo^{4+}. The coexistence of AFM and FM interactions in the frustrated magnet may be the origin of spin glass.

Funding Information This work was supported by the National Nature Science Foundation of China through Grant No. U1809215 and the Zhejiang Provincial Natural Science Foundation of China through Grant No. LY18E020016.

References

1. Greedan, J.E.: Geometrically frustrated magnetic materials. J. Mater. Chem. **11**(1), 37–53 (2000)
2. Harris, M.J., Bramwell, S.T., Mcmorrow, D.F., Zeiske, T., Godfrey, K.W.: Geometrical frustration in the ferromagnetic pyrochlore $Ho_2Ti_2O_7$. Phys. Rev. Lett. **79**(13), 2554–2557 (1997)
3. Attig J., Trebst S., Classical spin spirals in frustrated magnets from free-fermion band topology. Phys. Rev. B 96,085145 (2017)
4. Lacroix, C., Mendels, P., Mila, F.: Introduction to Frustrated Magnetism. Springer, Berlin Heidelberg (2011)
5. Gingras, M.J.P., Stager, C.V., Raju, N.P., Gaulin, B.D., Greedan, J.E.: Static critical behavior of the spin-freezing transition in the geometrically frustrated pyrochlore antiferromagnet $Y_2Mo_2O_7$. Phys. Rev. Lett. **78**(5), 947–950 (1997)
6. Gardner, J.S., Dunsiger, S.R., Gaulin, B.D., Gingras, M.J.P., Greedan, J.E., Kiefl, R.F., Lumsden, M.D., MacFarlane, W.A., Raju, N.P., Sonier, J.E., Swainson, I., Tun, Z.: Cooperative paramagnetism in the geometrically frustrated pyrochlore antiferromagnet $Tb_2Ti_2O_7$. Phys. Rev. Lett. **82**(5), 1012–1015 (1999)
7. Fukazawa H., Melko R., Higashinaka R., Maeno Y., Gingras M., Magnetic anisotropy of the spin-ice compound $Dy_2Ti_2O_7$. Phys. Rev. B 65(5), 054410 (2002)

8. Ying, Y., Wang, L., Li, W., Qiao, L., Zheng, J., Yu, J., Cai, W., Jiang, L., Che, S., Zhang, L., Ling, L.: Spin glass in a geometrically frustrated magnet of $ZnFe_2O_4$ nanoparticles. J. Supercond. Nov. Magn. 31, 3553 (2018)
9. Greedan, J.E., Sato, M., Yan, X., Razavi, F.S.: Spin-glass-like behavior in $Y_2Mo_2O_7$, a concentrated, crystalline system with negligible apparent disorder. Solid State Commun. **59**(12), 895–897 (1986)
10. Miyoshi, K., Nishimura, Y., Honda, K., Fujiwara, K., Takeuchi, J.: Magnetic ordering of pyrochlore oxides $R_2Mo_2O_7$ (R=Er–Nd, Y) by AC and DC magnetic measurements. Phys. B Condens. Matter. 284(7), 1463–1464 (2000)
11. Raju, N.P., Gmelin, E., Kremer, R.K.: Magnetic-susceptibility and specific-heat studies of spin-glass-like ordering in the pyrochlore compounds $R_2Mo_2O_7$ (R=Y, Sm, or Gd). Phys. Rev. B. **46**(9), 5405 (1992)
12. Dunsiger, S.R., Kiefl, R.F., Chow, K.H., Gaulin, B.D., Gingras, M.J.P., Greedan, J.E., Keren, A., Kojima, K., Luke, G.M., Macfarlane, W.A.: Muon spin relaxation investigation of frustrated antiferromagnetic pyrochlores A2B2O7. Hyperfine Interact. 104(1–4), 275–280 (1997)
13. Gardner, J.S., Ehlers, G., Bramwell, S.T., Gaulin, B.D.: Spin dynamics in geometrically frustrated antiferromagnetic pyrochlores. J. Phys. Condens. Matter. 16(11), S643 (2004)
14. Taguchi, Y., Ohgushi, K., Tokura, Y.: Optical probe of the metal-insulator transition in pyrochlore-type molybdate. Phys. Rev. B. 65(11), 115102 (2002)
15. Dunsiger, S.R., Kiefl, R.F., Chow, K.H., Gaulin, B.D., Gingras, M.J.P., Greedan, J.E., Keren, A., Kojima, K., Luke, G.M., Macfarlane, W.A.: Low temperature spin dynamics of geometrically frustrated antiferromagnets $Y_2Mo_2O_7$ and $Y_2Mo_{1.6}Ti_{0.4}O_7$ studied by muon spin relaxation. J. Appl. Phys. 79(8), 6636–6638 (1996)
16. Gardner, J.S., Gingras, M.J.P., Greedan, J.E.: Magnetic pyrochlore oxides. Rev. Mod. Phys. 82(1), 53–107 (2010)
17. Gingras, M.J.P., Stager, C.V., Gaulin, B.D., Raju, N.P., Greedan, J.E.: Nonlinear susceptibility measurements at the spin-glass transition of the pyrochlore antiferromagnet $Y_2Mo_2O_7$. J. Appl. Phys. 79(8), 6170–6172 (1996)
18. Silverstein, H.J., Fritsch, K., Flicker, F., Hallas, A.M., Zhou, H.D.: Liquidlike correlations in single-crystalline $Y_2Mo_2O_7$: an unconventional spin glass. Phys. Rev. B. 89(5), 188–192 (2014)
19. Arrott, A.: Criterion for ferromagnetism from observations of magnetic isotherms. Phys. Rev. 108(6), 1394–1396 (1957)
20. Lamichhane, T.N., Taufour, V., Thimmaiah, S., Parker, D.S., Bud'Ko, S.L., Canfield, P.C.: A study of the physical properties of single crystalline Fe_5B_2P. J. Magn. Magn. Mater. 401, 525–531 (2015)
21. Meschede, D., Steglich, F., Felsch, W., Maletta, H., Zinn, W.: Specific heat of insulating spin-glasses, (Eu,Sr)S, near the Onset of Ferromagnetism. Phys. Rev. Lett. 44(2), C345–C347 (1980)
22. Wenger, L.E., Keesom, P.H.: Calorimetric investigation of a spin-glass alloy: CuMn. Phys. Rev. B. 13(9), 4053–4059 (1976)